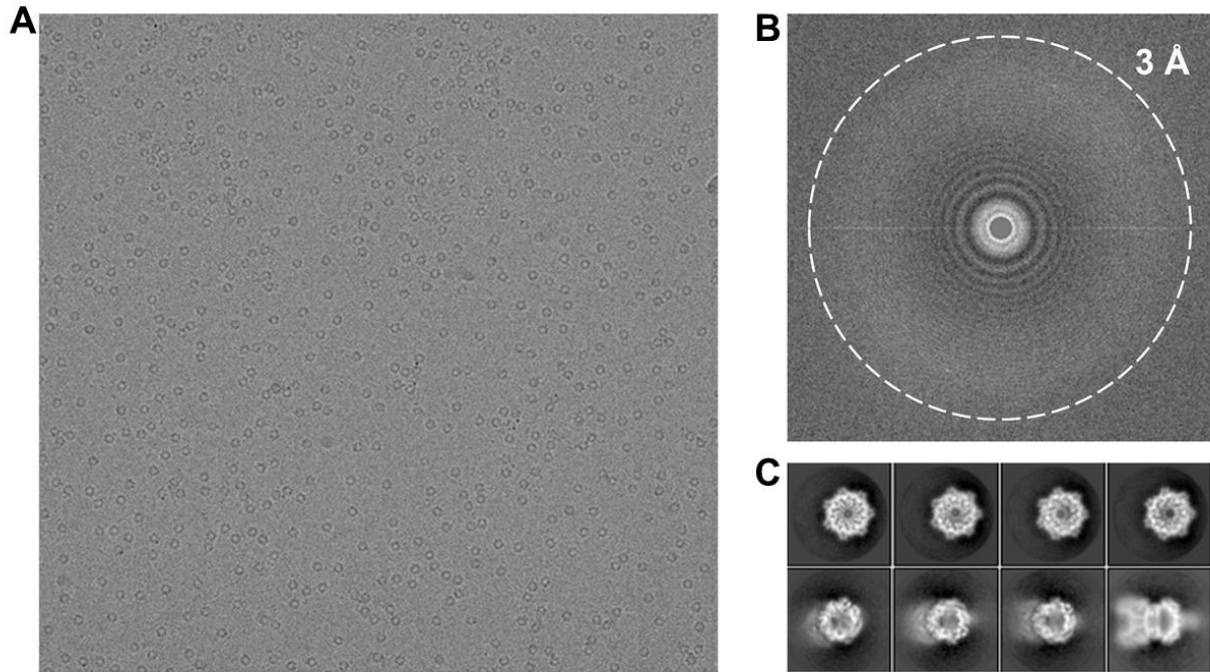


## Supporting information

### Supplementary Figures



**Fig. S1. A representative micrograph collected with Titan Krios and K2 camera**

- A.** A representative YnaI Cryo-EM image after motion correction. The particles show a strong preferred orientation.
- B.** Fourier transform of the image shown in (a). The dash cycle indicates the 3Å resolution in the Thon ring.
- C.** The 2D class averages of the Cryo-EM dataset. The upper row shows the top view classes and the lower row shows the tilt and side view classes.

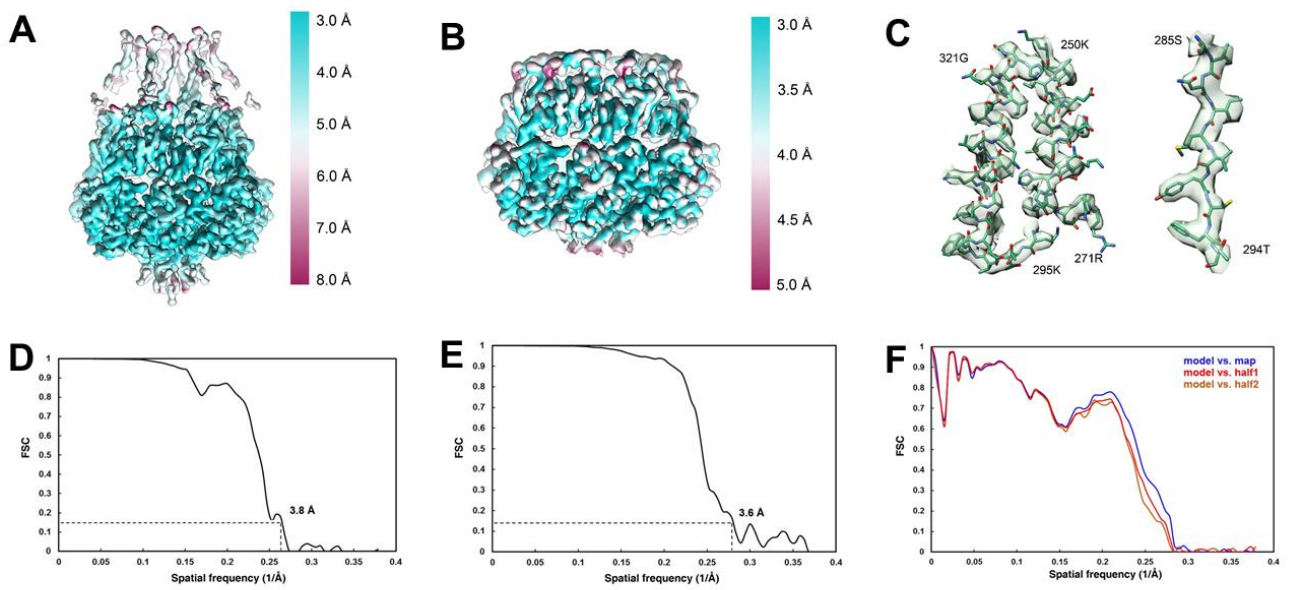


**Fig. S2. Local resolution maps and FSC curves**

**A-B.** The local resolution map of the overall structure (a) and the intracellular domain structure (b) refined within a soft mask.

**C.** The Cryo-EM densities of the selected region were superimposed with the atomic model.

**D-E.** The FSC curve of the overall refinement (a) and the intracellular domain refinement (b) within a soft mask.

**F.** The FSC curve of the intracellular domain atomic model cross-validation.

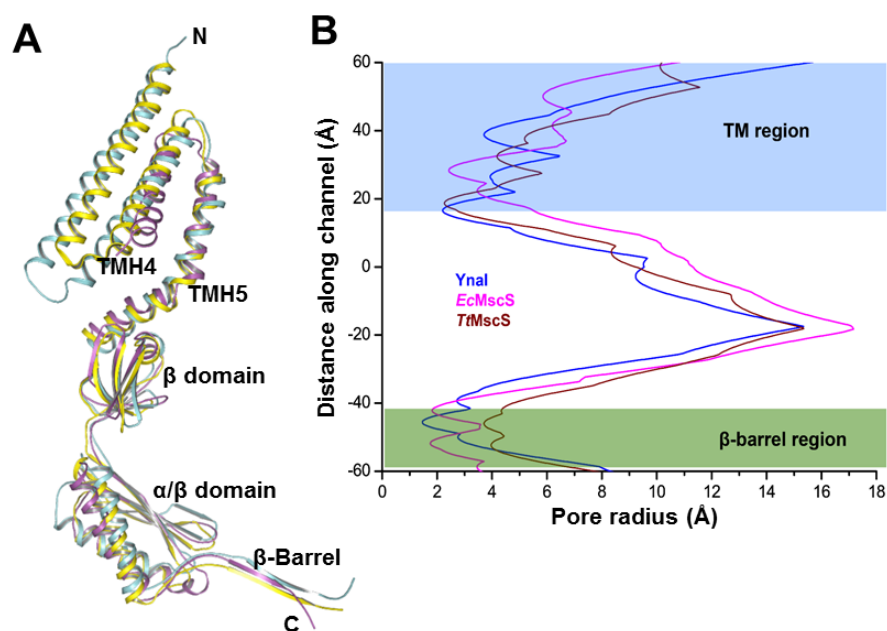


**Fig. S3. Overview structure of YnaI in the closed conformation**

- A.** YnaI in a closed conformation. Stereo views of structural alignment of one single YnaI protomer with *TtMscS* (Protein Data Bank code: 3UDC) and closed state of *EcMscS* (Protein Data bank code: 2OAU). Protomers of YnaI, *TtMscS* and *EcMscS* are shown in purple, cyan and yellow, respectively.
- B.** Plots of pore radiuses of YnaI, *TtMscS* and *EcMscS*, shown in blue, magenta and brown colors, respectively.

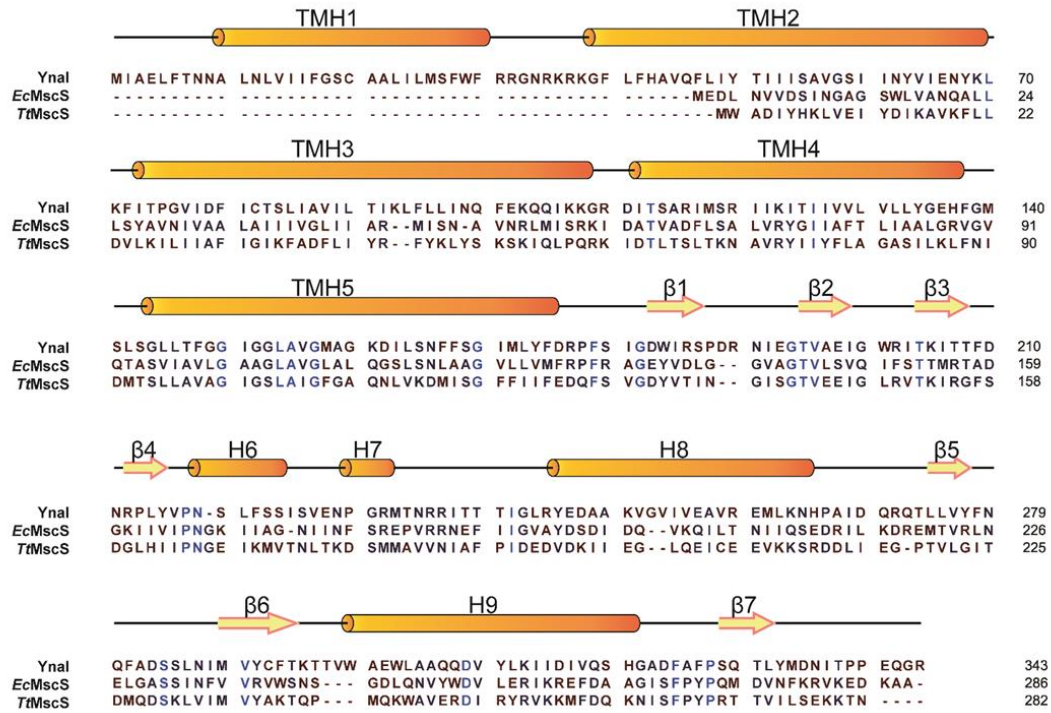


**Fig. S4. YnaI contains five TMHs**

Sequence alignment of YnaI, *TtMscS* and *EcMscS*. Conserved residues are highlighted in blue.

Secondary structural elements of YnaI are indicated above the sequence.

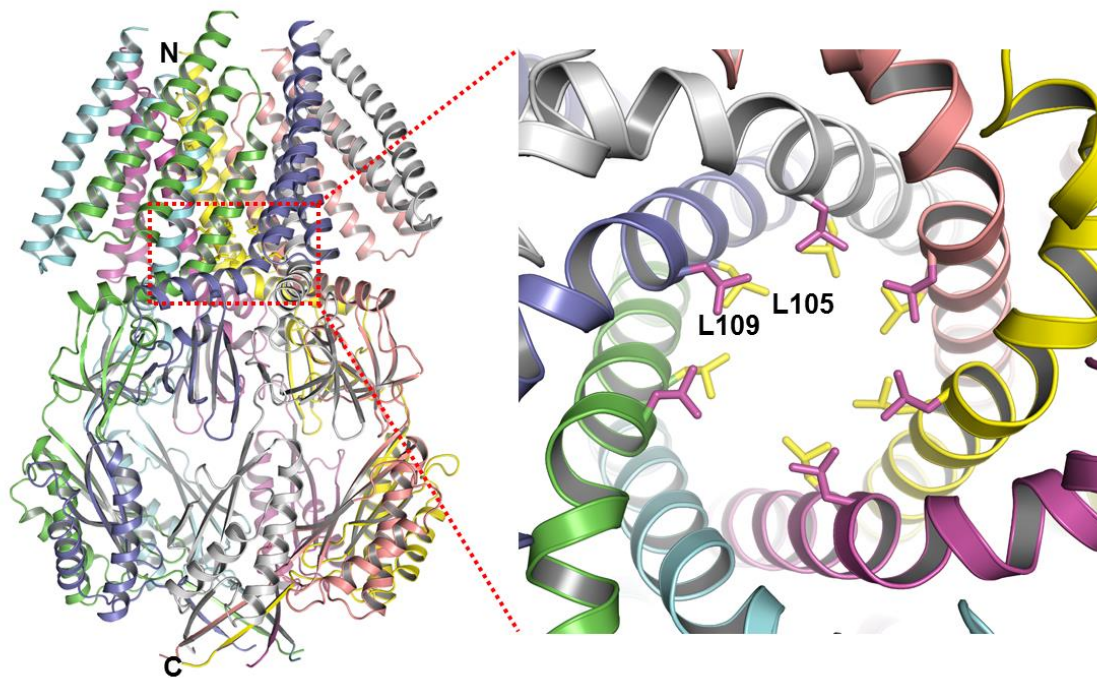


**Fig. S5. The *EcMscS*<sup>L105</sup> and *EcMscS*<sup>L109</sup> residues gate the channel**

Left: Cartoon represents the overall structure of *EcMscS* homoheptamer. Different subunits are shown in different colors.

Right: The *EcMscS*<sup>L105</sup> and *EcMscS*<sup>L109</sup> residues locate at the gating site of this channel as indicated in left panel. The *EcMscS*<sup>L105</sup> and *EcMscS*<sup>L109</sup> residues are shown in yellow and magenta sticks and indicated, respectively.

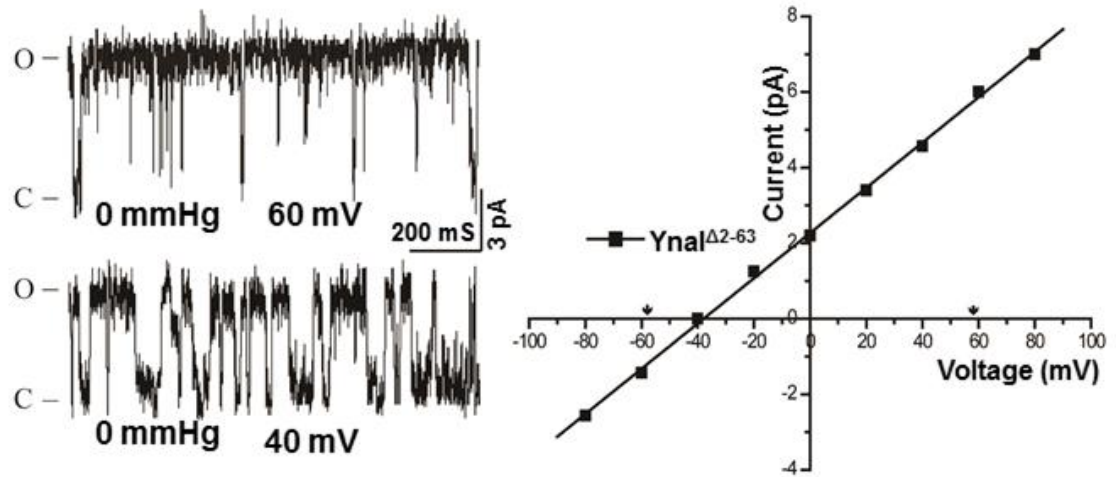


**Fig. S6. TM1 and TM2 of YnaI are responsible for gating the channel**

Left: spontaneous current traces recorded at +40 mV and +60 mV from the YnaI $\Delta^{2-63}$  mutant without application of pressure. Right: I-V curves for the YnaI $\Delta^{2-63}$ . The reversal potential measured from the I-V curve was  $-39.2 \pm 0.6$  mV ( $n = 5$ , mean  $\pm$  SE).

## Supplementary Tables

**Table S1. Calculated quantum chemical and thermodynamic energies for the process  $A + (\text{H}_3\text{CSCH}_3)_7 \rightarrow A@(\text{H}_3\text{CSCH}_3)_7$  ( $A = \text{Na}^+, \text{K}^+, \text{F}^-, \text{Cl}^-, \text{NO}_3^-$ )**

Ion types (A)	$\Delta E_e/\text{kcal}\cdot\text{mol}^{-1}$	$\Delta E_0/\text{kcal}\cdot\text{mol}^{-1}$	$\Delta H/\text{kcal}\cdot\text{mol}^{-1}$	$\Delta G/\text{kcal}\cdot\text{mol}^{-1}$
<b>Na<sup>+</sup></b>	<b>-8.65</b>	<b>-8.85</b>	<b>-9.09</b>	<b>-0.87</b>
<b>K<sup>+</sup></b>	<b>-2.50</b>	<b>-3.17</b>	<b>-3.09</b>	<b>3.51</b>
<b>F<sup>-</sup></b>	<b>-32.59</b>	<b>-31.78</b>	<b>-32.24</b>	<b>-23.31</b>
<b>Cl<sup>-</sup></b>	<b>-22.32</b>	<b>-22.02</b>	<b>-21.90</b>	<b>-16.56</b>
<b>NO<sub>3</sub><sup>-</sup></b>	<b>-23.50</b>	<b>-22.54</b>	<b>-21.85</b>	<b>-13.83</b>

\*  $E_e$  and  $E_0$  denote the calculated quantum mechanical energies at the equilibrium structures and the ones corrected with zero-point energies. H and G are the enthalpies and Gibbs free energies calculated at 298 K and 101.325 kPa (1 atm).

**Table S2. Property summary of YnaI, YnaI<sup>M158A</sup> and YnaI<sup>Δ2-63</sup> in different solutions in this study**

<b>Proteins</b>	<b>Solvents</b>	<b>Vrev (mV)</b>	<b>Px/Py</b>	<b>Conductance (r, pS)</b>	<b>n</b>
<b>YnaI</b>	<b>KCl</b>	<b>-39.2±0.5</b>	<b>8.9±0.3</b>	<b>43±0.34</b>	<b>5</b>
	<b>KF</b>	<b>-19.2±1.6</b>	<b>2.6±0.2</b>	<b>66±6.12</b>	<b>4</b>
	<b>KNO<sub>3</sub></b>	<b>-52.3±0.4</b>	<b>39.6±5.0</b>	<b>216±16.6</b>	<b>4</b>
<b>YnaI<sup>M158A</sup></b>	<b>KCl</b>	<b>-26.5±1.9</b>	<b>4±0.5</b>	<b>108.6±29.7</b>	<b>6</b>
	<b>KF</b>	<b>-28.2±2.6</b>	<b>4.5±0.7</b>	<b>135.3±44.7</b>	<b>6</b>
	<b>KNO<sub>3</sub></b>	<b>-35.1±0.5</b>	<b>6.6±0.2</b>	<b>99.3±12.5</b>	<b>7</b>
<b>YnaI<sup>Δ2-63</sup></b>	<b>KCl</b>	<b>-39.2±0.6</b>	<b>9.0±0.5</b>	<b>82.9±2.98</b>	<b>5</b>
	<b>KF</b>	<b>-14.4±1.7</b>	<b>2.0±0.2</b>	<b>52.2±2.2</b>	<b>4</b>
	<b>KNO<sub>3</sub></b>	<b>-51.9±0.8</b>	<b>39.3±4.7</b>	<b>156.3±16.23</b>	<b>4</b>

The reversal potential (Vrev) and conductance were measured through the I-V curve. The applied negative pressures were monitored by piezoelectric pressure transducer (World Precision Instruments).